Nonlinear Dyn
https://doi.org/10.1007/s11071-018-4359-y

ORIGINAL PAPER

When underwater degraded images meet logical stochastic resonance

Nan Wang · Bing Zheng · Haiyong Zheng · Biao Yang

Received: 22 February 2018 / Accepted: 13 May 2018

Abstract Owing to light attenuation and high background noise, underwater images are significantly degraded, which hiders the development of underwater exploration. However, noise itself can be used to counter noise. In this paper, we apply logical stochastic resonance (LSR) to help detect weak objects from low-quality underwater images. On the basis of analysis of the physical character of underwater images, three models, namely basic dynamical system driven by Gaussian noise, basic dynamical system driven by Ornstein–Uhlenbeck (OU) noise, and dynamical system with extra delay loop, are chosen to study the performance of LSR-based object detection. The main workflow of LSR-based object detection is introduced. To analyze the performance of LSR, we perform explicit experiments and systematically discuss the interplay of additional noise with the system parameters. LSR is proven to be helpful in detecting weak objects from low-quality underwater images. Both OU noise and extra delay loop will help the whole system to maintain stability in a higher noisy background.

Keywords Logical stochastic resonance · Weak object detection · Underwater image processing

1 Introduction

The intricacies presented by the underwater environment are far more complicated than those by the terrestrial environment [1]. The radiance of underwater objects is highly attenuated and is usually overwhelmed by the background noise, making visually based underwater object detection difficult [2,3]. Classical image pre-processing methods, such as denoising and contrast enhancement, cannot obtain good effects in processing such degraded images [3,4]. Thus, a specific method that can handle the underwater weak object detection is badly needed. Underwater object detection is by nature weak signal detection. Underwater weak object detection is possible by conducting theoretical study on the physical character of the original signal and then processing using a corresponding method.

The most difficult part in processing underwater image is the high-intensity background noise and low signal-to-noise ratio (SNR). To counter the high-intensity background noise, the use of stochastic resonance (SR) is quite intuitive. SR is the most significant noise-useable theory [5]. In the last decades, SR has proven its usefulness in different kinds of information

This work was supported by National Natural Science Foundation of China (No. 61703381), Natural Science Foundation of Shandong Province (No. ZR2017BF006), China Postdoctoral Science Foundation (No. 2016M590658) and Fundamental Research Funds for the Central Universities (No. 201713017).

N. Wang (✉) · B. Zheng · H. Zheng
Ocean University of China, Qingdao 266100, China
N. Wang
e-mail: wangnanseu@163.com

B. Yang
ChangZhou University, Changzhou 213164, China

Published online: 23 May 2018

systems [6], such as electrical systems [7], biological systems [8], and neural networks [9]. SR has been also used to enhance the image quality. For example, Fleischer et al. recovered noise-hidden images in a self-focusing medium [10]. Monifi et al. reported chaos-induced SR in an optomechanical system [11]. Jha et al. used SR to realize noise-induced contrast enhancement on singular values [12]. More applications, such as feature extraction in low-quality fingerprint images [13], logo extraction [14], and magnetic resonance image enhancement [15], have also been reported.

With the development of SR research, some extension performances have also been studied, including noise-induced resonance [16], coherence resonance [17], and ghost resonance [18]. Among the explorations, logical stochastic resonance (LSR) is an importance branch. LSR allows a nonlinear system to work as a reliable logical element to give logical output of weak input, with the help of moderate noise [19,20]. Although this is a young theory, it attracts immense attention from researchers and is useful in different kinds of applications, ranging from noise-freed LSR [21,22], LSR in synthetic genetic networks [23,24], to LSR in triple-well potential system [25]. Given that the detection problem is logical, LSR may be suitable for dealing with such a problem. However, how to design the LSR nonlinear system corresponding to the typical background noise character is still an open problem. Back to the underwater image object detection issue, optimal LSR system designation should refer to the complicated underwater ambient surrounding. To analyze the interplay of background noise with the LSR system, the present work discusses three LSR models, namely the popular classical quartic-bistable dynamical system subjected to Gaussian noise, the quartic-bistable dynamical system subjected to Ornstein–Uhlenbeck (OU) noise, and the dynamical system with extra delay loop. The goal is to propose an optimal system which can accurately detect weak objects in degraded underwater images.

The rest of this paper is organized as follows. In Sect. 2, the underwater light propagation process is systematically analyzed and three different nonlinear dynamics are introduced. In Sect. 3, the main frame of the LSR-based image object detection and experiment approach are described. In Sect. 4, the explicit experimental results are presented. Finally, the conclusions of the study are elaborated in Sect. 5.

2 General model

2.1 Basic dynamical system

Given that this study is only focused on object detection and extraction from a heavy noise background, only two logical states (0 and 1) are needed. We consider logic 0 as the background and logic 1 as the object. With these two states, we choose the popular quartic-bistable dynamical system [26] as the base nonlinear system, which is governed by (1):

$$U(x) = \frac{b}{4}x^4 - \frac{a}{2}x^2 - rx, \tag{1}$$

where $U(x)$ represents the bistable potential system. a and b are the coefficients of linear and nonlinear terms, respectively. When the bias r is zero, the system (1) has two stable states at $x_{\pm} = \pm\sqrt{a/b}$ and a potential barrier with $\Delta V = a^2/4b$ at $x = 0$. r has the effect of asymmetrizing the two potential wells to achieve different output logics.

Figure 1 shows the potential well of system (1) with different bias r. when the bias r is changed, the bistable states become asymmetric and the potential barrier is changed. When the potential well is symmetric and the barrier is not high, the particles jump arbitrarily between the two wells under the effect of additional power offered by the noise. However, according to Langevin dynamics, if the potential well is not symmetric, the particles have a greater likelihood of jumping into and staying in the low-potential well. Thus, by helping the corresponding pixels jump to the tuned right potential well, we can detect the weak signal and manage the output logic according to specific applications at the same time.

2.2 MODEL1: basic dynamical system driven by Gaussian noise

When the system is driven by a weak signal subjected to Gaussian white noise, the Langevin function of (1) can be written as follows:

$$\dot{x} = \dot{U}(x) + I(t) + D\eta(t), \tag{2}$$

with the nonlinear system $U(x)$ is given by (1), $\eta(t)$ denotes the Gaussian white noise with autocorrelation

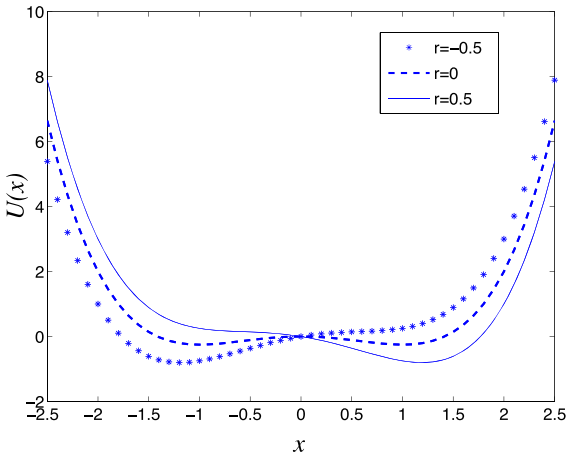

Fig. 1 The potential $U(x)$ for different bias r

function $\langle \eta(t)\eta(0)\rangle = 2D\delta(t)$, and D is the strength of the noise. $I(t)$ is the low-amplitude input signal. $t\,(t \geq 0)$ is the index of sampling. When $I(t)$ is a time-varying signal, t can represent the sampling time. When $I(t)$ represents an image signal, t can be considered as the pixel coordinate.

2.3 MODEL2: basic dynamical system driven by OU noise

In most cases, the additive noise is considered to have a correlation length shorter than any other length scale in the systems, so that it can be represented as delta correlated. However, this idealization has never been realized in the real physical world. Particularly, underwater researchers have proposed that the ambient noise affects the imaging in a correlated way [27]. Therefore, colored noise should be considered as having a constructive role underwater. The current work opts to study OU noise to explore the influence of noise inherent correlation effect on the system result.

The basic dynamical system is still (1). When it is driven by the original signal subjected to OU noise, the Langevin function can be written as:

$$\dot{x} = \dot{U}(x) + I(t) + y(t), \tag{3}$$

where $U(x)$ is (1), and $I(t)$ has the similar meaning with (2). The noise $y(t)$ is an OU stochastic process driven by Gaussian white noise with zero mean and

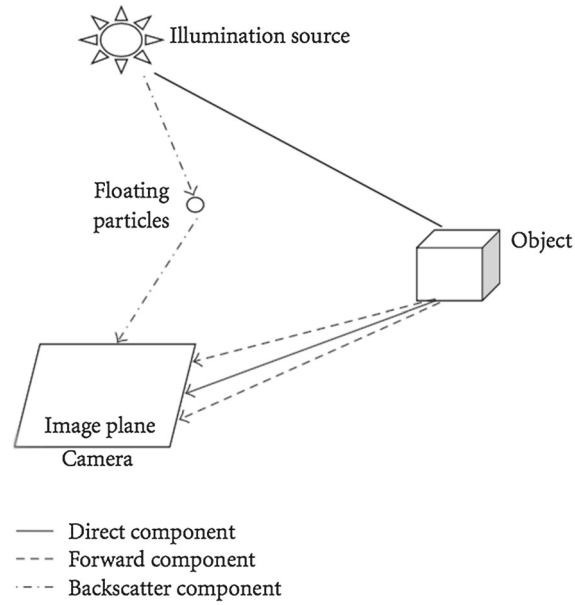

Fig. 2 The three components of underwater optical imaging: direct component (straight line), forward component (dashed line), and backward scatter component (dash-dot line)

delta correlation.

$$\dot{y} = -\frac{y}{t_c} + \frac{\sqrt{2D}}{t_c}\eta(t) \tag{4}$$

where $\eta(t)$ and D are like (2). The OU noise $y(t)$ therefore possesses the correlation

$$\langle y(t)y(s)\rangle = \frac{D}{t_c}\exp(-|t-s|/t_c) \tag{5}$$

which approaches the case of white noise as correlation length $t_c \to 0$.

2.4 MODEL3: basic dynamical system with extra delay loop

The degraded effect of underwater images is composed of absorption and scattering effect. Scattering effect is more complicated than absorption and can be further decomposed as backward scattering and forward scattering. Figure 2 shows the typical light propagation situation in water. Specifically, backward scattering effect is mainly induced by the ambient underwater environment, which can be modeled as inherent noise. Forward component is related to object reflect. Hence, it is much

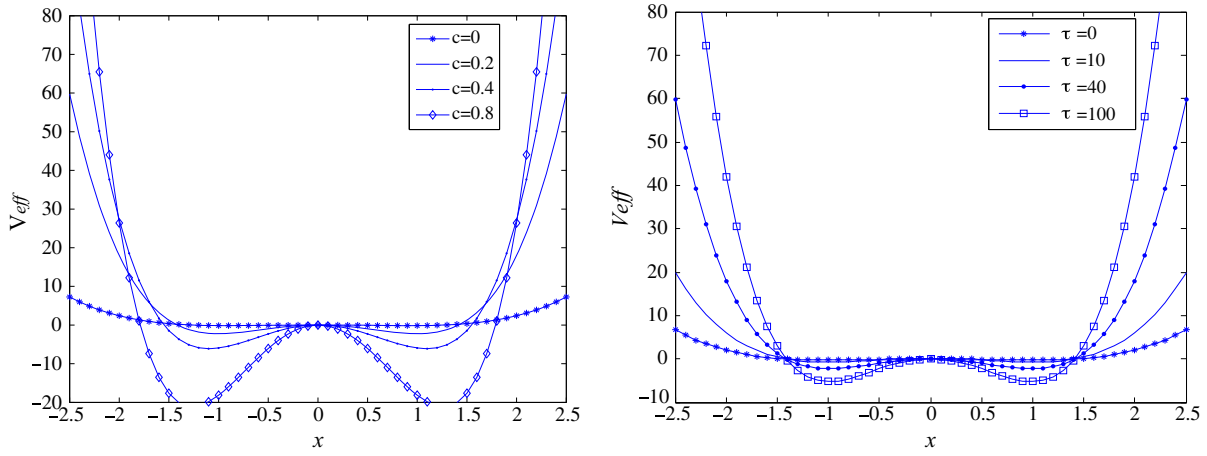

Fig. 3 **a** The effective potential of equation (7) for different c with $\tau = 40$. **b** The effective potential of equation (7) for different delay lengths τ with $c = 0.2$

more complicated and correlated with the real object signal. In our model, this effect is simulated as an extra delay loop that is correlated to the neighbor radiance.

The bistable nonlinear system with extra delay loop can be described by the following Langevin equation

$$\dot{x} = -V^{'}(x(t), x(t-\tau)) + r + I(t) + \eta(t), \qquad (6)$$

$V^{'}(x(t), x(t-\tau))$ is the derivative of the symmetric double-well potential with a delay component, which is given by

$$V(x(t), x(t-\tau)) = \frac{b}{4}x(t)^4 - \frac{a}{2}x(t)^2 - \frac{c}{2}x(t-\tau)^2 \quad (7)$$

where c is the weight of linear delay. Other parameters have the same meaning as (2). The effective potential of (7) is plotted in Fig. 3.

3 Main framework of the LSR-based object detection

Our objectives are to explore the effects of the three aforementioned LSR systems on the weak object detection in degraded underwater images and find the relationship between background noise and LSR system components. To realize these aims, we first provide the main workflow of LSR-based object detection. The three major processing steps are:

1. Dimensional reduction, which means reducing the original 2D image to a 1D form signal;
2. Normalization, which means normalizing the original signal to [0, 1];
3. Passing the dynamical system. This process will provide a logical output, where 0 means the background pixel and 1 means the object pixel, or vice versa.

The main framework of LSR-based object detection is shown in Fig. 4.

Figure 5 shows a group of original images captured in fresh river water from different distances of the object board to the camera and the corresponding detection results for different models. The object board is a picture of a wheel, which is 1.3 cm × 1.3 cm in size, with each line width at 1 mm. The camera is a 411000-pixel CCD sensor. The water attenuation and absorption coefficients, measured by an AC-S meter (WET-LABS), are 4.5 m^{-1} and 1.3 m^{-1}, respectively. Figure 5 clearly shows that in a long distance range, all the three models can help to detect the weak object from the degraded raw images. When the useful information is completely overwhelmed by the surrounding noise (distance=30 cm), the output images of the LSR system do not show a clear shape. In this situation, the result of LSR system with extra delay loop is much clearer than the other models. Besides, the width of the detection result of the OU driven model is wider than that of the

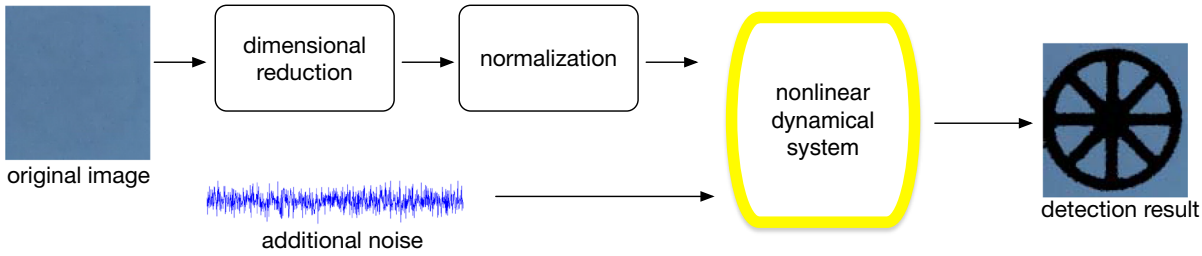

Fig. 4 The main framework of LSR-based object detection

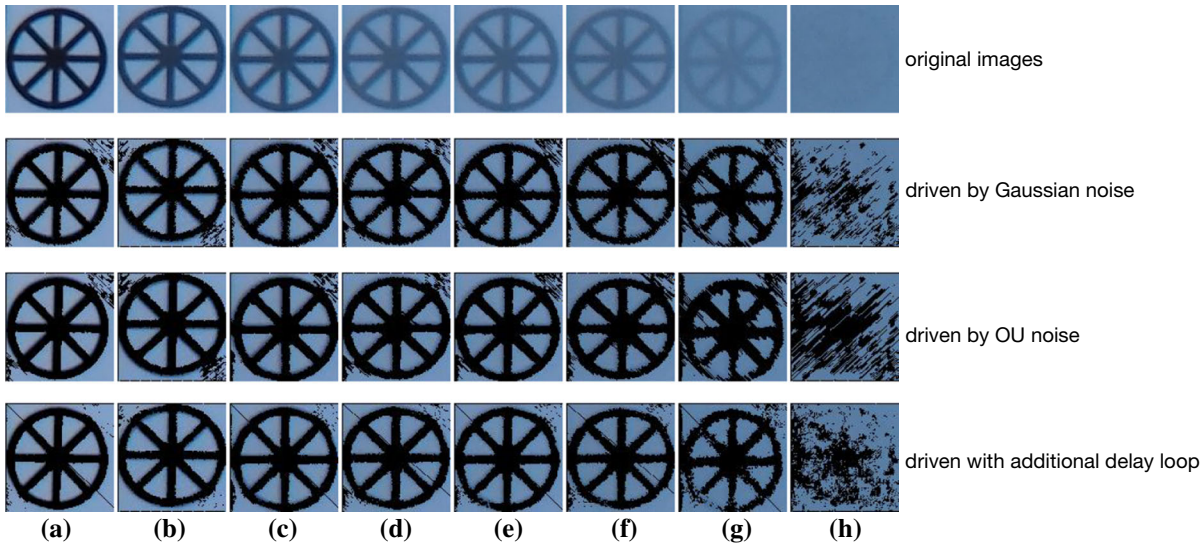

Fig. 5 Images of a picture of a wheel in fresh river water from different distances and the corresponding detection results used different LSR models. The distance from object board to the camera is **a** 12.5 cm, **b** 15 cm, **c** 17.5 cm, **d** 20 cm, **e** 22.5 cm, **f** 25 cm, **g** 27.5 cm, and **h** 30 cm, respectively. The parameters of the three models are set particularly to show the best performance of each model using the aforementioned method

other two models. The number of fake detection points of the extra delay loop model is the lowest.

To obtain the best detection performance, setting the parameters of the system correctly is necessary. In practice, three parameters, a, b and r, are available to modulate the nonlinear basic bistable system. The ratio of a and b is essentially important. According to Kramers' rate [28], the noise-induced hopping between the local equilibrium states is $\frac{1}{\sqrt{2\pi}} \exp(-\frac{\triangle V}{D})$, and $\triangle V = a^2/4b$. This means the detection scale is decided by the ratio of a and b. Meanwhile, the logic function of the whole system is dependent on r. Therefore, r should be chosen according to the actual situation of the object picture. In this study, we first set $a = 1.25$, $b = 1$, and $r = 0.3$ empirically to acquire an asymmetric bistable potential well.

The strength of the additional noise D has a huge effect on whether or not the system can obtain LSR and realize the optimum state. It should be set in accordance with the intensity of the background noise. How the other parameters of OU noise and delay loop affect the performance of the whole system will be studied explicitly below. Besides, the main computation cost of the LSR-based method lies in the numerical iteration to solve the differential equation. In this work, we use four-step Runge–Kutta method.

4 Experiment results

The probability of obtaining an accurate detection result is calculated to analyze the performance of LSR and the effect of parameters D, t_c, and τ on the result of underwater image detection. As all the models can obtain almost the same clear results when the distance from the camera to object board is nearer than 25 cm, in this paper, we choose the images captured at much further distances (distance $\geq$ 25 cm) as the research object to perform the explicit experiments. At the same time, the other group of experiment images using a photograph of resolution lines is added as the object board to study the resolution power of the three models. To compare the detection result, the truth value of every photograph is manually and carefully labeled. To guarantee the validity, this step is performed with the help of ground truth images. The raw images and corresponding truth-value images are shown in Fig. 6.

The correct probability P for each cropped picture is obtained by comparing the detection results with the truth-value image. Two auxiliary ratios are calculated. One is the ratio of object, as

$$P_o = \frac{n_o}{n_{ot}}, \tag{8}$$

where n_o is the number of pixels correctly detected as the object the result image. n_{ot} is the total number of pixels labeled as object in the truth-value image. The other one is

$$P_b = \frac{n_b}{n_{bt}}, \tag{9}$$

where n_b is the number of pixels correctly detected as the background in the result image. n_{bt} is the total number of pixels labeled as background in the truth-value image.

Then, P is obtained as

$$P = \epsilon P_o + (1 - \epsilon) P_b. \tag{10}$$

Here, ϵ is the normalization weight to modulate the degree of importance of P_o and P_b. In this experiment, as we mainly aim to detect the object, we set $\epsilon = 0.8$.

Figure 7 shows the changing curves of correct detection probability P versus the additional noise intensity D of the six different images shown in Fig. 6. The correct detection probability P is calculated by the aforementioned method.

First, we focus separately on the changing trend of the three models. When the LSR system is driven with Gaussian noise (red line), the correct probability first increases and then decreases as the noise intensity amplifies, except when $distance = 30$ cm, the correct detection probability P decreases monotonously with the increasing additional noise intensity. A typical LSR phenomenon is obtained. The same phenomenon is also observed when an extra delay loop is added to the system (green line). The correct detection results of the LSR system driven with OU noise are more stable (blue line). A non-monotonous trend is not obtained. With the amplification of noise intensity, the correct probability slowly increases, which means that, in this set of system parameters, a higher OU noise is needed to obtain high detection probability correctly. Although the correct probability of the system driven by OU noise changes monotonously in Fig. 7, if we analyze the functions of P, D, and t_c as a whole, a non-monotonous performance can be observed (Fig. 8).

When the three models are compared, except for $distance = 30$ cm, the peak points of the three models occur from left to right as follows: the peak of the system driven with Gaussian noise appears first, followed by the peak of the system with additional delay loop, and then the peak of system driven by OU noise appears last. This order means that small extra turbulence power is needed to obtain the optimal performance when the system is driven by Gaussian noise; more is needed when the system has an extra delay loop, and the most power is needed for the system driven by OU noise.

The sequence of the best detection performance is as follows: LSR system driven by Gaussian noise is better than LSR driven by OU noise, and LSR system driven by OU noise performs better than LSR system with extra delay loop. However, this order is not always the case. The curves exhibited in Fig. 7 are obtained when we set $a = 1.25$, $b = 1$, $r = 0.3$, $t_c = 0.1$, $c = 0.45$, and $\tau = 10$. This set of system coefficients is not the optimal for the different models. Thus, although the system with extra delay loop looks like it obtained lower accuracy probability in Fig. 7, it may perform better in other sets of system parameters. Therefore, the comparison of best performance of the models in the figure has no meaning. We only focus on the tendency of the changing of each model.

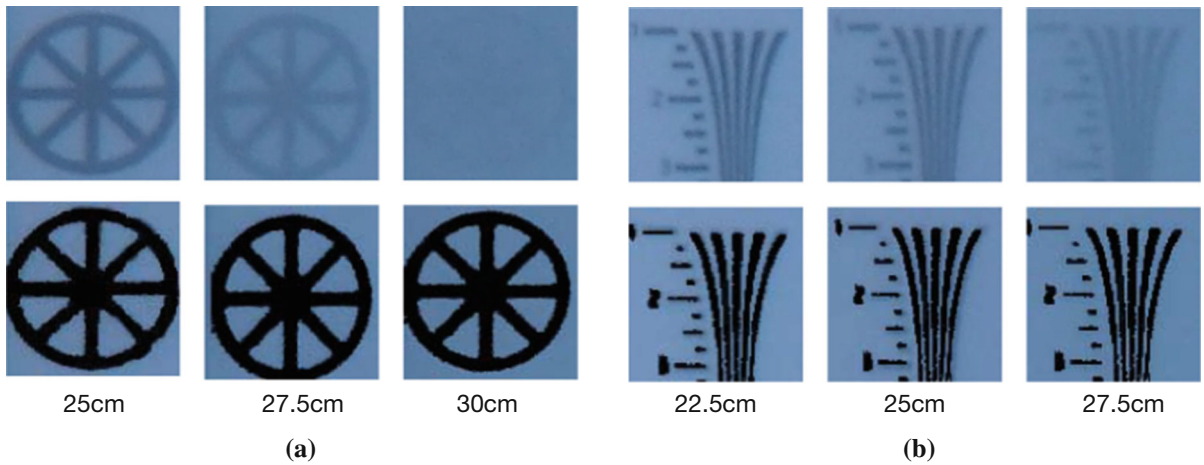

Fig. 6 **a** Images of a picture of a wheel in fresh river water at different distances and the corresponding manually labeled truth-value images. **b** Images of a picture of resolution lines in fresh river water at different distances and the corresponding manually labeled truth-value images

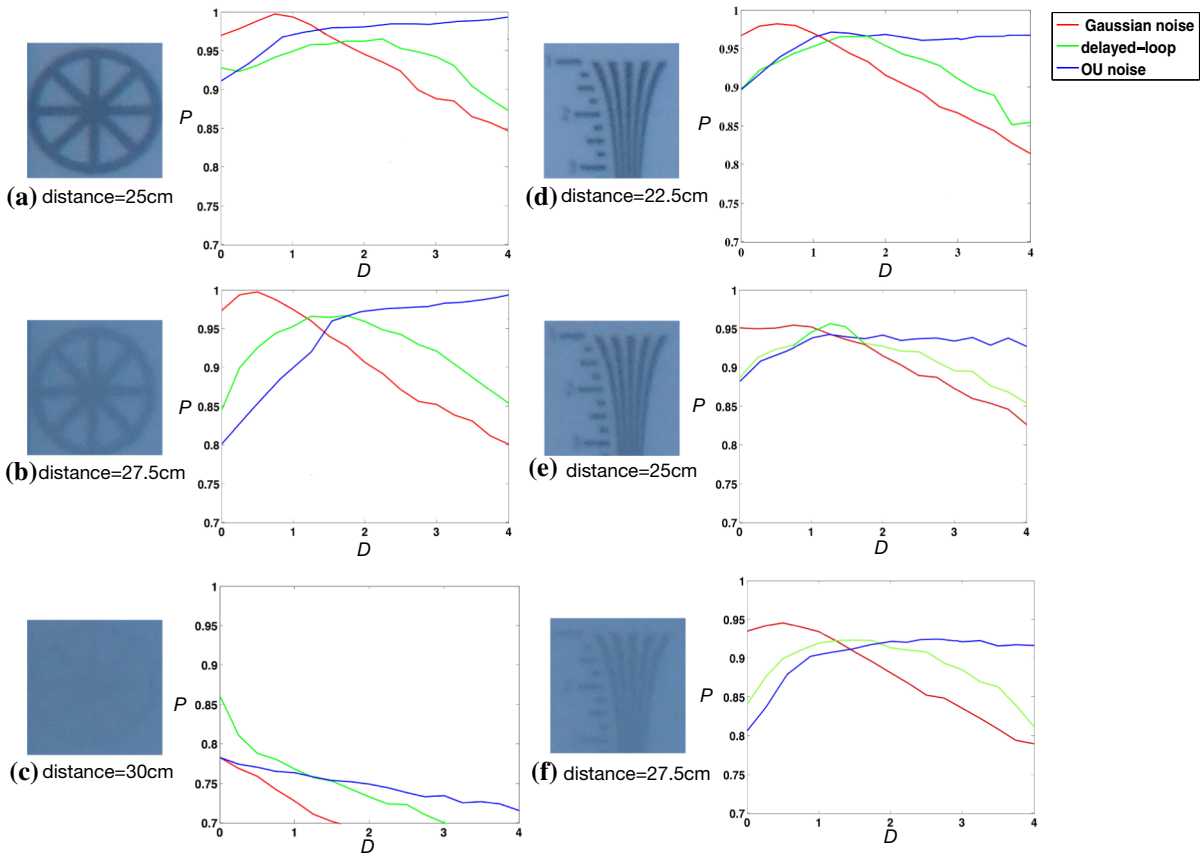

Fig. 7 The changing curve of correct detection probability P versus the additional noise intensity D for the three models. Here, the parameters are set as $a = 1.25$, $b = 1$, $r = 0.3$, $t_c = 0.1$, $c = 0.45$, and $\tau = 10$.

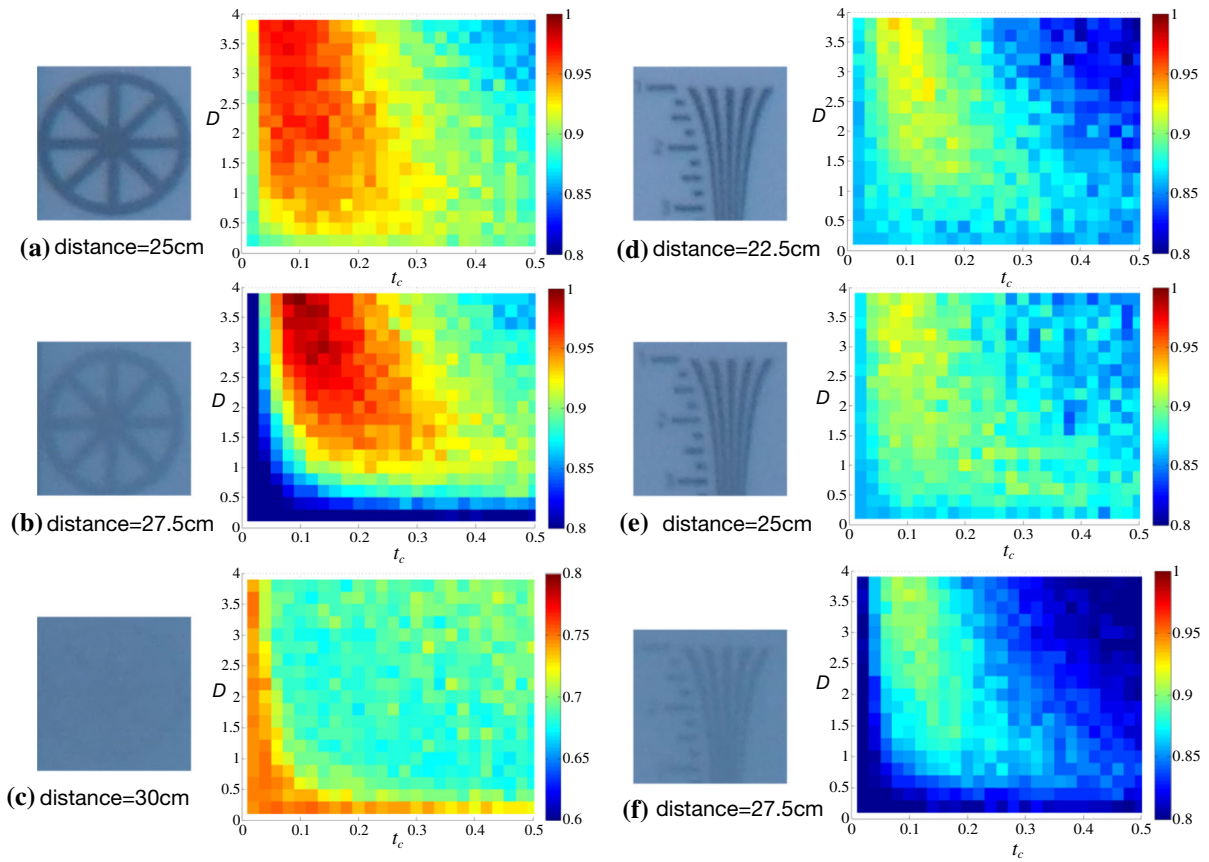

Fig. 8 The correct probability P map versus both noise intensity D and correlation length t_c when the system is driven by OU noise. Here, the corresponding system parameters are set as $a = 1.25$, $b = 1$, and $r = 0.2$

Third, it is clear from Fig. 7 that when the distance from the object to the camera is 30 cm (Fig. 7c), the useful information is completely attenuated and overwhelmed by the background noise. Even with the help of the powerful human brain, the shape in such an image cannot be identified. For such highly degraded image, detection probability above 70% is obtained with the help of a nonlinear system. This means such nonlinear systems work better than human eyes to detect weak objects in highly degraded underwater images. An analysis of the changing tendency of P–D of the three models reveals that the peak of correct probability decreases with the increase in noise intensity. The peak of correct probability is approximately 85% by the system with extra delay loop. No LSR phenomenon is observed because the background noise is much higher than the intensity of the weak signal, which means no extra turbulence power is needed in such a situation.

Moreover, a comparison of the performance of the two original image groups, namely wheel shape and resolution lines, indicates that the maximum correct probability of the images of resolution lines is a little lower than that of the images of the wheel shape, even for the same distance. This finding is attributed to the changing interval space among the resolution lines. The resolution lines are sparse in the upper part and tight in the bottom part. When the interval space is smaller than the detection scale of the LSR system, the resolution lines may not be detected separately, but as a whole. Therefore, the error rate may increase. Determining how to enhance the detection scale is still an open question.

As previously mentioned, it is very important to note that, except for the additional noise intensity D, other coefficients may affect the final correct detection probability. Take OU noise as example, where the correlation length t_c is also very important. To analyze the

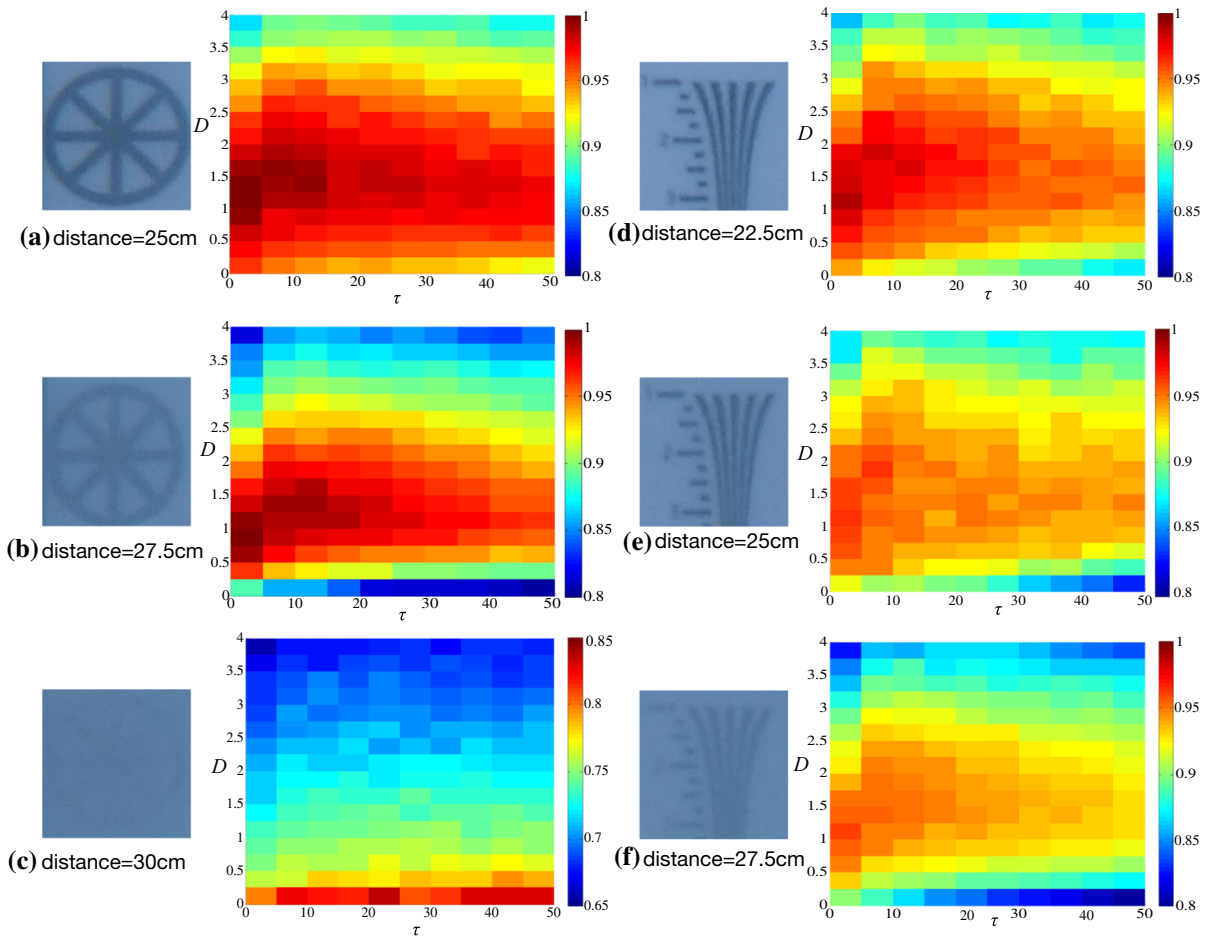

Fig. 9 The correct probability P map versus both noise intensity D and correlation length t_c when the system is added with extra delay loop. Here, the corresponding system parameters are set as $a = 0.85$, $b = 1$, $r = -0.05$, and $c = 0.45$

effect of OU noise on the detection result, we plot the correct probability map versus both noise intensity D and correlation length t_c as Fig. 8. With the exception of Fig. 8c, the detection performance clearly changes non-monotonously with the increase in correlation length, which first increases to the peak point and then decreases. In addition, when the correlation length is short ($t_c < 0.2$), the detection probability slowly increases with the increase in the noise intensity, an outcome that is in accordance with the tendency curve in Fig. 7. When the correlation length is long ($t_c > 0.2$), increasing the intensity of OU noise will also lead to the LSR phenomenon.

Meanwhile, we also plot the correct probability map versus both noise intensity D and delay length τ for the system with extra delay loop in Fig. 9. Clearly, when the system has an extra delay loop, almost 100% correct detection probability may be obtained in a wide range of D and τ. When the intensity D is smaller than 1.5, the detection probability is slowly decreases with the increase in the delay length. In such scenario, the extra delay loop may ruin the performance of the system. However, when the intensity D is larger than 1.5, the detection performance changes non-monotonously with the increase in delay length, which first increases to the peak point and then decreases. Specially, Fig. 9c shows that an extra delay loop may help to obtain better detection performance when the raw image is highly degraded. In such situation, an extra delay loop is really an effective help.

5 Conclusion

This work proposes a LSR-based weak object detection method from low-quality underwater images. On the basis of the physical character of underwater light propagation, we introduce three LSR models, namely basic bistable system driven by Gaussian noise, basic bistable system driven by OU noise, and bistable system with extra delay loop, to study the effectiveness of LSR-based weak object detection. Systematical experiments are performed, and both the correct detection probability P versus the additional noise intensity D and other corresponding parameters in the three models are provided.

It is proved that with the help of LSR, a weak object can be detected in a wide range of distance. Even when the original image is difficult for humans to distinguish, the shape of the weak object can be recognized after processing by the LSR system. Both OU noise and extra delay loop will help to maintain good performance in increased additional noise.

Visually based underwater object detection is a long-standing hard problem. With the help of LSR theory, underwater exploration may embrace a new development. However, this method also has several drawbacks. For example, the resolution scale of the LSR-based detection problem is not well handled, a topic which should be researched further in the future study.

Compliance with ethical standards

Conflicts of interest The authors declare that they have no conflict of interest concerning the publication of this manuscript

References

1. Duntley, S.Q.: Light in the sea. JOSA **53**(2), 214 (1963)
2. Raimondo, S., Silvia, C.: Underwater image processing: state of the art of restoration and image enhancement methods. EURASIP J. Adv. Signal Process. **2010**(1), 1–15 (2010)
3. Jaffe, J.S.: Underwater optical imaging: the past, the present, and the prospects. IEEE J. Ocean. Eng. **40**(3), 683 (2015)
4. Chiang, J.Y., Chen, Y.C.: Underwater image enhancement by wavelength compensation and dehazing. IEEE Trans. Image Process. **21**(4), 1756 (2012)
5. Benzi, R., Sutera, A., Vulpiani, A.: The mechanism of stochastic resonance. J. Phys. A Math. Gen. **14**(11), 453 (1981)
6. Chen, H., Varshney, L.R., Varshney, P.K.: Noise-enhanced information systems. Proc. IEEE **102**(10), 1607 (2014)
7. Harmer, G., Davis, B., Abbott, D.: A review of stochastic resonance: circuits and measurement. IEEE Trans. Instrum. Meas. **51**(2), 299 (2002)
8. Hnggi, P.: Stochastic resonance in biology how noise can enhance detection of weak signals and help improve biological information processing. Chemphyschem A Eur. J. Chem. Phys. Phys. Chem. **3**(3), 285 (2002)
9. Mitaim, S., Kosko, B.: Adaptive stochastic resonance in noisy neurons based on mutual information. IEEE Trans. Neural Netw. **15**(6), 1526 (2004)
10. Dylov, D.V., Fleischer, J.W.: Nonlinear self-filtering of noisy images via dynamical stochastic resonance. Nat. Photonics **4**(5), 323 (2010)
11. Monifi, F., Zhang, J., Özdemir, Ş.K., Peng, B., Liu, Y., Bo, F., Nori, F., Yang, L.: Optomechanically induced stochastic resonance and chaos transfer between optical fields. Nat. Photonics **10**(6), 399 (2016)
12. Jha, R.K., Chouhan, R.: Noise-induced contrast enhancement using stochastic resonance on singular values. Signal Image Video Process. **8**(2), 339 (2014)
13. Ryu, C., Kong, S.G., Kim, H.: Enhancement of feature extraction for low-quality fingerprint images using stochastic resonance. Pattern Recognit. Lett. **32**(2), 107 (2011)
14. Jha, R.K., Biswas, P.K., Shrivastava, S.: Logo extraction using dynamic stochastic resonance. Signal Image Video Process. **7**(1), 119 (2013)
15. Rallabandi, V.P., Roy, P.K.: Magnetic resonance image enhancement using stochastic resonance in Fourier domain. Magn. Reson. Imag. **28**(9), 1361 (2010)
16. Yang, J.H., Sanjun, M.A.F., Liu, H.G., Zhu, H.: Noise-induced resonance at the subharmonic frequency in bistable systems. Nonlinear Dyn. **87**(3), 1721 (2017)
17. Hu, B., Kurths, J., Zhou, C.: Array-enhanced coherence resonance. Nature **437**(7059), 601 (2001)
18. Rajamani, S., Rajasekar, S., Sanjuán, M.A.F.: Ghost-vibrational resonance. Commun. Nonlinear Sci. Numer. Simul. **19**(11), 4003 (2014)
19. Murali, K., Rajamohamed, I., Sinha, S., Ditto, W.L., Bulsara, A.R.: Realization of reliable and flexible logic gates using noisy nonlinear circuits. Appl. Phys. Lett. **95**(19), 194102 (2009)
20. Murali, K., Sinha, S., Ditto, W.L., Bulsara, A.R.: Reliable logic circuit elements that exploit nonlinearity in the presence of a noise floor. Phys. Rev. Lett. **102**(10), 194102 (2009)
21. Gupta, A., Sohane, A., Kohar, V., Murali, K., Sinha, S.: Noise-free logical stochastic resonance. Phys. Rev. E Stat. Nonlinear Soft Matter Phys. **84**(2), 055201 (2011)
22. Yang, B., Zhang, X., Luo, M.: When noise-free logical stochastic resonance occurs in a bistable system. Nonlinear Dyn. **87**(3), 1957 (2017)
23. Sharma, A., Kohar, V., Shrimali, M.D., Sinha, S.: Realizing logic gates with time-delayed synthetic genetic networks. Nonlinear Dyn. **76**(1), 431 (2013)
24. Wang, N., Song, A.: Enhanced logical stochastic resonance in synthetic genetic networks. IEEE Trans. Neural Netw. Learn. Syst. **27**(12), 2736 (2016)
25. Zhang, H., Yang, T., Xu, W., Xu, Y.: Effects of non-Gaussian noise on logical stochastic resonance in a triple-well potential system. Nonlinear Dyn. **76**(1), 649 (2014)

26. Kohar, V., Murali, K., Sinha, S.: Enhanced logical stochastic resonance under periodic forcing. Commun. Nonlinear Sci. Numer. Simul. **19**(8), 2866 (2014)
27. Wang, G., Zheng, B., Sun, F.F.: Estimation-based approach for underwater image restoration. Opt. Lett. **36**(13), 2384(2011)
28. Gammaitoni, L., Hänggi, P., Jung, P., Marchesoni, F.: Stochastic resonance. Rev. Mod. Phys. **70**(1), 223 (1998)